

Spatial-aware Vision Language Model for Autonomous Driving

Weijie Wei^{1,2,*}Zhipeng Luo^{1,†}¹MotionalLing Feng¹Venice Erin Liong^{1,‡}²University of Amsterdam

Abstract

While Vision-Language Models (VLMs) show significant promise for end-to-end autonomous driving by leveraging the common sense embedded in language models, their reliance on 2D image cues for complex scene understanding and decision-making presents a critical bottleneck for safety and reliability. Current image-based methods struggle with accurate metric spatial reasoning and geometric inference, leading to unreliable driving policies. To bridge this gap, we propose LVLD (LiDAR-Vision-Language), a novel framework specifically designed to upgrade existing VLMs with robust 3D metric spatial understanding for autonomous driving by incorporating LiDAR point cloud as an extra input modality. A key challenge lies in mitigating the catastrophic disturbance introduced by disparate 3D data to the pre-trained VLMs. To this end, we introduce a Gradual Fusion Q-Former that incrementally injects LiDAR features, ensuring the stability and preservation of the VLM's existing knowledge base. Furthermore, we develop a spatial-aware question-answering (SA-QA) dataset to explicitly teach the model advanced 3D perception and reasoning capabilities. Extensive experiments on driving benchmarks demonstrate that LVLD achieves superior performance compared to vision-only counterparts across scene understanding, metric spatial perception, and reliable driving decision-making. Our work highlights the necessity of explicit 3D metric data for building trustworthy VLM-based autonomous systems.

1. Introduction

Large vision-language models (VLMs) have recently emerged as a promising foundation for end-to-end autonomous driving systems. By coupling visual perception with language-native reasoning and explanation, VLM-based agents can describe scenes, justify decisions, and expose intermediate rationales that were opaque in earlier pipelines [24, 38, 42, 43]. However, despite rapid progress, a critical limitation persists: contemporary VLMs predominantly consume 2D imagery and thus struggle with metric spatial

*Work done as an intern at Motional. †Project lead. ‡Corresponding author.

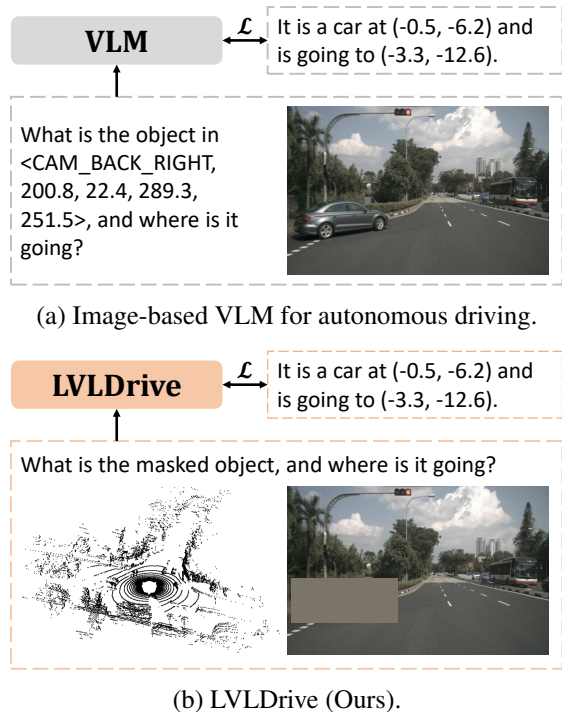


Figure 1. (a) Typical image-based VLMs take only images as input and train the LLM through image-conditioned question answering. In contrast, our LVLD leverages both image and LiDAR inputs and incorporates carefully designed spatial-aware QAs to encourage effective LiDAR integration and enhance spatial understanding.

understanding—precise distances, extents, occlusions, and interactions in 3D. These capabilities are not optional; they are prerequisites for safe planning in dense, multi-agent urban scenes, especially in autonomous driving. Recent benchmarks that isolate spatial queries corroborate this gap, showing that strong general-purpose VLMs underperform on driving-critical spatial reasoning tasks [46, 57].

Why is this challenging? Inferring geometry from monocular or multi-view images is ill-posed under occlusions, adverse weather, and viewpoint changes. Even when bird's-eye-view (BEV) features or video context are introduced, image-only models tend to confuse appearance with metric structure, leading to brittle estimates of range, free space, and collision risk. As a result, VLM-based driving agents

may produce fluent rationales yet fail at the quantitative spatial inferences that underwrite reliable control. LiDAR offers a complementary pathway. Its calibrated 3D point measurements provide direct, long-range, and lighting-invariant geometric cues for scene layout, drivable area, and inter-agent relations. Prior works have demonstrated that integrating LiDAR with images can significantly enhance the perception performance in autonomous driving scenes [28, 51]. While integrating LiDAR with VLMs seems like a natural next step, it remains challenging. Pre-trained VLMs are optimized on massive image–text corpora but not on LiDAR–image–text multimodal data. Consequently, naively injecting a disparate 3D representation can severely disrupt their learned alignments, resulting in suboptimal linguistic competence and visual grounding.

To this end, we introduce LVLDdrive (LiDAR–Vision–Language), a framework designed to equip VLMs with robust 3D metric spatial understanding capabilities while preserving their learned knowledge, as shown in Fig. 1. The key component is a Gradual Fusion Q-Former structure that incrementally injects LiDAR embeddings into the VLM via a gated attention mechanism. Rather than exposing the model to unaligned 3D signals from LiDAR at once, LVLDdrive schedules the introduction of LiDAR embeddings over training, allowing the model to adapt its cross-modal attention without drifting from its original visual–linguistic manifold. The trainable gate learns when—and how strongly—to rely on LiDAR, enabling graceful fallback to image cues when 3D observations are sparse or noisy. To explicitly enforce spatial reasoning and encourage the integration of LiDAR features, we further construct SA-QA dataset, a spatial-aware visual question–answering dataset derived from ground-truth 3D annotations in standard driving scenes. To explicitly enforce spatial reasoning and promote the integration of LiDAR features, we construct SA-QA, a spatial-aware visual question–answering dataset derived from ground-truth 3D annotations in standard driving scenes. The dataset focuses on metric and relational question–answer pairs that are central to autonomous driving, pairing linguistically natural questions with unambiguous, 3D-grounded answers and complementing prior instruction-tuned driving corpora [10, 43, 50]. In addition, a subset of question–answer pairs incorporates a modality-masking mechanism that forces the VLM to rely on LiDAR information, thereby promoting the alignment between LiDAR and image representations.

We evaluate LVLDdrive on recent language–based driving benchmarks emphasizing spatial reasoning and decision reliability. Across scene understanding, metric spatial perception, and planning-relevant intent prediction, LVLDdrive consistently outperforms vision-only VLM baselines, narrowing the gap between the commonsense strengths of VLMs and the metric precision demanded by safety-critical driving. By

integrating LiDAR in a stability-preserving manner and supervising with spatial-aware language tasks, our approach improves the reliability of LLM-based autonomous systems and underscores the necessity of explicit 3D metric cues for trustworthy end-to-end driving. The contributions of this work are threefold: (1) we introduce LVLDdrive, augmenting a pre-trained VLM with a Gradual Fusion Q-Former to incrementally inject LiDAR embeddings while preserving visual–linguistic priors; (2) we construct a spatial-aware QA dataset (SA-QA) on top of the nuScenes dataset and its ground-truth annotations, to boost the spatial understanding and reasoning of LVLDdrive; (3) we conduct extensive experiments and ablation studies to quantify the performance gains and to clarify how LiDAR injection and fine-tuning on our proposed spatial-aware dataset contribute to faithful 3D spatial reasoning.

2. Related Work

Language–Driving Datasets. Early efforts grounded natural-language commands and explanations in real driving scenes—e.g., Talk2Car [9] for referred-object commands, the BDD-X [23] explanation corpus, and BDD-OIA [55] for object-induced action with textual rationales. More recently, driving QA resources have scaled markedly: nuScenes-QA [40] standardized multi-view urban driving VQA, while LingoQA [36] scaled short video scenarios with human truthfulness judging. Graph-structured chain-of-thoughts reasoning for driving was introduced by DriveLM [43], which released DriveLM-Data on nuScenes and CARLA, and a GVQA protocol spanning perception, prediction, and planning. BEV-centric language benchmarks emerged to stress global scene and interaction reasoning (Talk2BEV-Bench [8], BEV-TSR [45] text-to-scene retrieval, ChatBEV-QA [54] with 137k questions). End-to-end language supervision also appears inside instruction datasets like NuInstruct [10] paired with BEV-Injected MLLMs. OmniDrive [50] proposed a holistic language–driving dataset with counterfactual reasoning. Most of the above datasets focus on generic driving scene understanding and decision-making. Recently, nuScenes-SpatialQA [46] benchmarked the spatial understanding capacity of various VLMs. While our SA-QA dataset is related in spirit, it focuses more on planning-oriented spatial reasoning and the modeling of interactions across LiDAR and vision modalities.

VLMs for Autonomous Driving. Vision-Language Models have been widely adopted in autonomous driving, predominantly using image inputs for tasks such as human-interpretable scene understanding and trajectory planning. For example, DriveLM [43] introduced a VLM-based “agent” performing joint graph VQA and end-to-end control; LMDrive [42] integrated LLM reasoning with closed-loop control; VLP [38] bridged perception, text, and planning

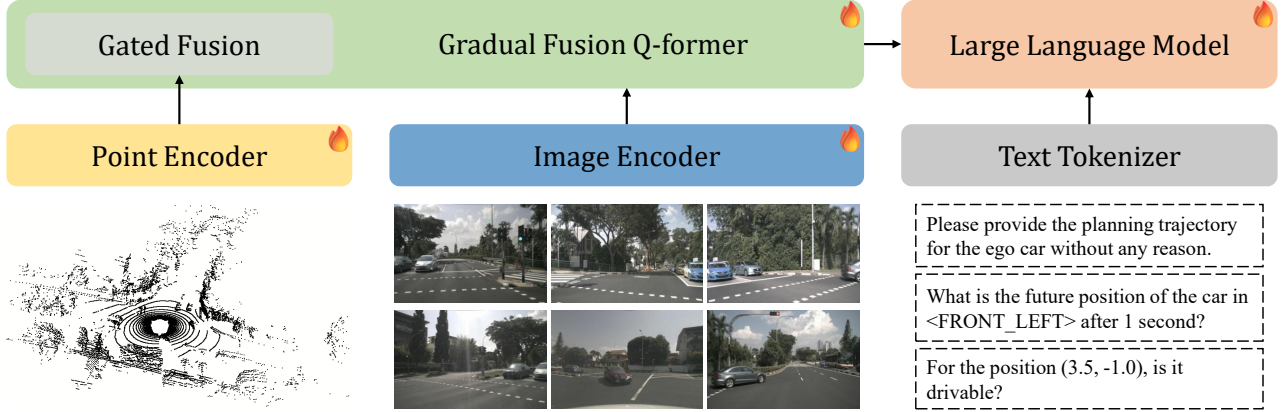


Figure 2. **Overview of LVLDdrive.** LVLDdrive takes text, images, and point clouds as multimodal inputs and employs three pretrained encoders, an LLM, and a Gradual Fusion Q-Former module that bridges visual and linguistic representations to generate task-specific responses. The fire symbol denotes trainable components.

with language supervision; and LLADA [24] adapted policies to new domains using LLM priors. GPT-style planners such as GPT-Driver [35] and DriveGPT4 [56] explored autoregressive action generation with rationales; DriveVLM [47] tailored MLLMs for driving QA and intent understanding; and DriVLM [19] built a video-language agent for interactive navigation. BEV-aware multimodal models like BEV-InMLLM [10] improved global spatial context, while V2X-VLM [59] leveraged infrastructure views. More recently, VLA families such as OpenDriveVLA [65] and AutoVLA [66] unified perception, reasoning, and action in a single autoregressive policy incorporating feasibility and physics constraints; InternDrive [63] focused on scenario understanding with MLLMs. Different from these image-based approaches, LiDAR-LLM [58] pioneers the use of LLMs for driving-scene understanding directly from LiDAR inputs, aiming to extend VLMs’ comprehension to more challenging real-world 3D scenes. In contrast, our work explores the complementary strengths of both image and LiDAR within a unified framework, leveraging the strong reasoning capabilities of pretrained VLMs together with the 3D metric information from LiDAR point clouds.

Spatial Understanding in VLMs. In recent years, generic VLMs [1, 20, 30, 52] have achieved remarkable progress, exhibiting strong reasoning and problem-solving abilities in open-ended tasks. However, several studies [21, 32, 34] have evaluated the spatial understanding and reasoning capabilities of VLMs and found they are far from satisfactory—even with enhancements such as chain-of-thought prompting [57]. To address these gaps, several recent studies on the understanding of indoor scenes—including SpatialVLM [4] and SpatialRGPT [7]—have explored fine-tuning strategies with spatially enriched task-specific datasets. In autonomous driving contexts, where accurate spatial reasoning is essential for planning and safety, benchmarking results on NuScenes-

SpatialQA [46] similarly reveals that current VLMs still fall short. These findings highlight the need to explore more capable approaches to effectively enhance spatial understanding and reasoning in autonomous driving scenarios.

3. Methodology

3.1. Preliminaries

Vision-Language Model (VLM). A VLM typically comprises three main components: a language model pretrained on large-scale text corpora using next-token prediction objectives [37, 48]; a vision encoder pretrained on visual tasks through self-supervised learning [3, 6, 17], contrastive learning [25, 41] or supervised learning [11, 16, 53]; and a projector that injects visual features into the language model. The projector can be a simple MLP, as in LLaVA [30, 31], or a more structured Q-Former [26] built with cross-attention layers. In the Q-Former, learnable queries attend to external visual features, enabling the model to retrieve and compress relevant information into a fixed-length of latent tokens. Since point cloud encoders yield variable-length outputs due to sparsity, we adopt a Q-Former-style projector to produce fixed-length token outputs, enabling robust interfacing with the language model.

Q-Former 3D Block. Q-Former 3D block is an upgraded version of the Q-Former and was proposed in OmniDrive [50]. While it shares the core idea and architecture of a standard Q-Former—*i.e.* two multi-head attention (MHA) layers per block stacked in depth—OmniDrive modifies the input formulation so that the architecture can decode object-centric features from images. As illustrated in Fig. 3, the first MHA layer in each block uses a shared set of learnable instance tokens as queries, keys, and values. Each query corresponds to a reference point in 3D space; thus, 3D positional embeddings derived from these reference points are

added to both the queries and keys. When a memory bank is available (carrying information from previous frames), memory tokens are concatenated to the keys and values to incorporate temporal context. The second MHA layer takes the output of the first layer as queries and the patch-wise image embeddings as keys and values, enabling retrieval and compression of visual features. Positional embeddings from the reference points are again added to the queries and keys to maintain spatial correspondence. Building on this design, OmniDrive further concatenates carrier tokens with the instance tokens and processes them through multiple Q-Former 3D blocks. The carrier tokens are then passed to the LLM, while the instance tokens are supervised with 3D perception objectives. Our fusion module is constructed on top of this Q-Former 3D block introduced by OmniDrive.

3.2. Framework Overview

As illustrated in Fig. 2, LVLDdrive takes text, images, and point clouds as multimodal inputs to generate task-specific responses via an LLM. The overall architecture comprises three pretrained encoders (for text, image, and point cloud), an LLM, and a Gradual Fusion Q-Former that serves as a projector between visual and linguistic representations. The text tokenizer, image encoder, LLM, and Gradual Fusion Q-Former—implemented with stacked multi-head attention blocks—have been jointly pretrained without point cloud input, enabling well-aligned feature representations across text-image modalities. This strong alignment, however, does not extend to the point cloud encoder. Unlike the image modality, large-scale LiDAR-text data for joint pretraining is scarce. This lack of alignment means that naively injecting point cloud features into the VLM could disrupt the well-learned text-image representations and lead to suboptimal performance. Our core challenge, therefore, is to effectively integrate these “out-of-domain” features under limited data conditions. To address this, we introduce a unified Gradual Fusion Q-Former that progressively integrates the newly acquired point cloud features into the carrier tokens and jointly retrieves multimodal representations for downstream reasoning.

3.3. Gradual Fusion Q-Former

As discussed in Sec. 3.2, a key challenge lies in how to inject point cloud features into an existing VLM where text and image representations are already well aligned. To address this, we investigate the Q-Former 3D block and identify its three inputs: 1) a set of learnable query tokens, 2) tokens from the memory bank, which encode object-centric features from historical frames, and 3) image feature tokens, through which information from the current frame is incorporated. Each token is associated with either a specific reference point in 3D space or a probability distribution over a set of reference points. These reference points are encoded as 3D

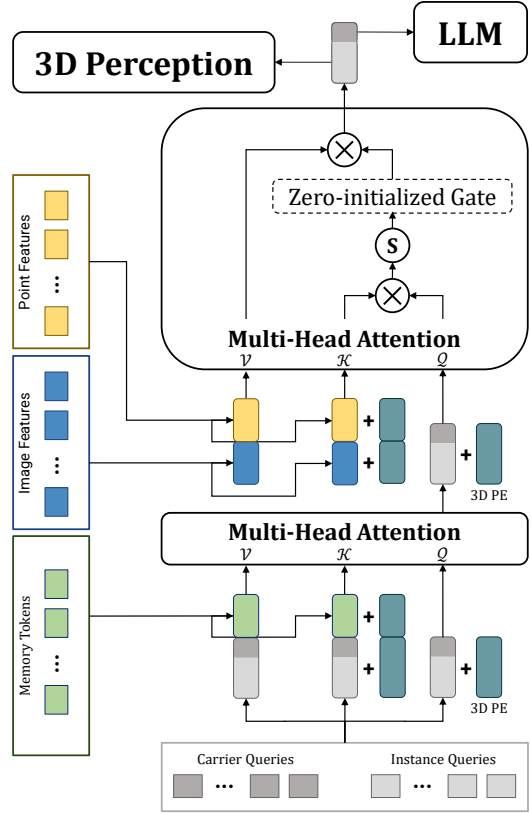


Figure 3. Gradual Fusion Q-Former. Each block contains two multi-head attention layers. The first layer uses learnable carrier and instance tokens as queries, keys, and values; the keys and values are extended with memory tokens when the memory bank is non-empty, and both queries and keys are augmented with 3D positional embeddings (3D PE) derived from reference points. The second layer introduces image and point features as keys and values, with queries and keys again augmented using their corresponding 3D positional embeddings. Note that the zero-initialized gate is applied only to point features. At the end of the module, the output queries are supervised by 3D perception objectives and LLM gradients separately.

positional embeddings, which are added to the tokens and actively participate in the attention computation.

To integrate point cloud features, a natural choice is to introduce them at the same stage as image features, while using the corresponding 3D locations as reference points for positional encoding. This leads to the architecture illustrated in Fig. 3. Through this design, we introduce an additional modality while preserving the sparse representation attribute of the Q-Former 3D block as well as its ability to leverage temporal information. However, we observe that naively introducing point cloud features in this manner destabilizes training and causes the model to converge to suboptimal optima. Inspired by LLaMA-Adapter [62], we therefore incorporate point cloud features through a zero-initialized gating mechanism.

Given a scene’s point cloud, image, and text prompt, we feed them into their respective encoders to obtain modality-specific representations, which are denoted as $F_P \in \mathbb{R}^{N_P \times C}$, $F_I \in \mathbb{R}^{N_I \times C}$ and $T \in \mathbb{R}^{N_T \times C}$, where N_P , N_I and N_T denotes the lengths of three modalities and C equals the feature dimension of the LLM. For Gradual Fusion Q-Former, the inputs to the first layer consist of learnable tokens $L \in \mathbb{R}^{N_L \times C}$ and memory tokens $M \in \mathbb{R}^{N_M \times C}$, where M is either inherited from the previous frame or zero-initialized when no preceding frame exists. The learnable tokens are then updated by the first layer as follows:

$$L \leftarrow \text{MHA} (L, [L; M], [L; M]) \quad (1)$$

where $\text{MHA}(\mathcal{Q}, \mathcal{K}, \mathcal{V})$ indicates a standard multi-head attention. When the pretraining starts with only the image modality available, the second layer of the Q-Former 3D block functions as a standard cross-attention layer and generates output as follows:

$$O_I = \text{MHA} (L, I, I) \quad (2)$$

In the joint training stage, we further introduce point features as additional keys and values to the second layer, as illustrated in Fig. 3. First, a set of linear layers is applied to transform the inputs into queries, keys and values:

$$\mathcal{Q} = \text{Linear}_q (L), \quad (3)$$

$$\mathcal{K}_I = \text{Linear}_k (F_I), \mathcal{K}_P = \text{Linear}_k (F_P), \quad (4)$$

$$\mathcal{V}_I = \text{Linear}_v (F_I), \mathcal{V}_P = \text{Linear}_v (F_P). \quad (5)$$

Then, the attention scores are calculated as:

$$S_I = \text{softmax} (\mathcal{Q} \mathcal{K}_I^T / \sqrt{C}), \quad (6)$$

$$S_P = \text{softmax} (\mathcal{Q} \mathcal{K}_P^T / \sqrt{C}) \quad (7)$$

where $S_I, S_P \in \mathbb{R}^{N_L \times N_C}$. Note that we add 3D positional embeddings derived from reference points to the queries, probability-accumulation-based 3D positional embeddings for each pixel to \mathcal{K}_I and 3D positional embeddings derived from each point feature’s spatial location to \mathcal{K}_P . By aligning the coordinate systems, all reference points reside in the same 3D physical space, enabling spatially aligned fusion. For clarity, these details are omitted from the formula in this section. The resulting scores are applied to the values to obtain the output:

$$O = \text{Linear}_o (S_I \mathcal{V}_I + S_P \mathcal{V}_P) \in \mathbb{R}^{N_L \times C}. \quad (8)$$

Since the point cloud features are newly introduced and have not yet been jointly trained with the image features or learnable tokens, they probably cause instability during the softmax operation. To this end, we introduce a zero-initialized learnable gate, denoted as g , to adaptively control the contribution of point cloud features during training:

$$O = \text{Linear}_o (S_I \mathcal{V}_I + \tanh(g) S_P \mathcal{V}_P) \in \mathbb{R}^{N_L \times C}. \quad (9)$$

Since g is zero-initialized, $\tanh(g)$ starts near zero, suppressing initially unaligned point features and allowing them to be gradually integrated into the Q-Former. This design preserves the training stability of the pre-existing components. To encourage diverse and complementary feature learning, we employ independent gates for each attention head, referred to as the multi-head gate in Tab. 3.

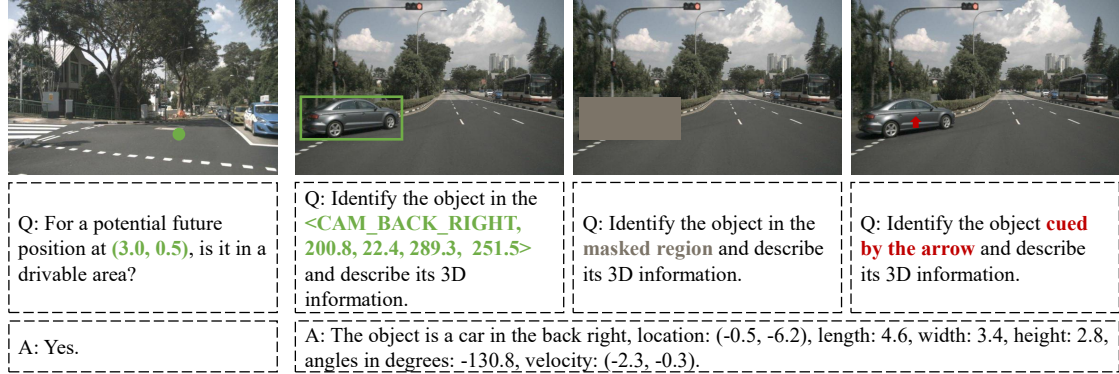
3.4. SA-QA Dataset

To enhance the spatial understanding capability of LVLDdrive and encourage its adaptation to LiDAR point cloud data, we construct the Spatial-Aware Question-Answering dataset, abbreviated as SA-QA. Built upon the nuScenes dataset [2], our SA-QA dataset encompasses both fundamental spatial perception questions and complex spatial reasoning tasks, as illustrated in Fig. 4.

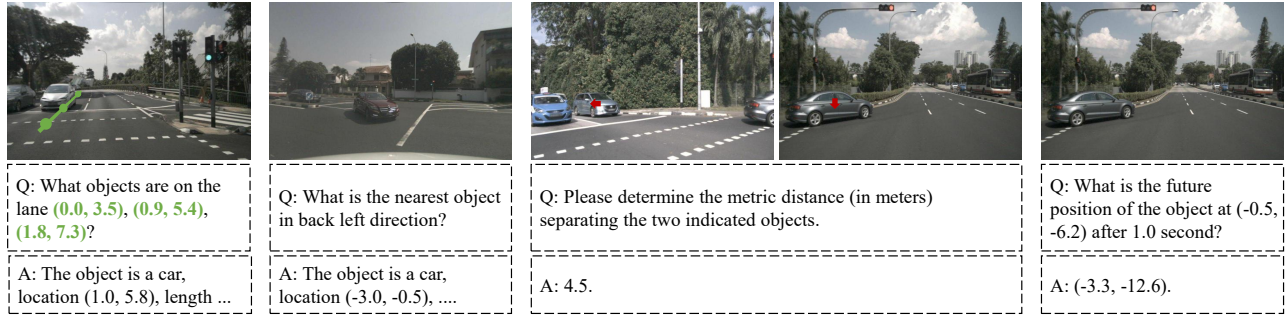
Spatial Perception. The spatial perception question-answering tasks in SA-QA can be categorized into two types. The first type asks whether a specific BEV point lies within a drivable area, allowing the language model to develop an awareness of road conditions. The second type requires the language model to identify an object in various ways and answer questions about its 3D attributes, including coordinates, size (length, width, and height), orientation, and velocity. In addition, we carefully design question-answer pairs to explicitly encourage the fusion of LiDAR and image features. For example, arrows in 2D images are used to indicate objects, prompting the model to perform cross-modal reasoning between images and point clouds. Similarly, masking the corresponding region in the 2D image forces the model to extract relevant information directly from the point cloud. Examples of spatial perception QAs are shown in Fig. 4(a).

Spatial Reasoning. Building upon the fundamental spatial perception tasks, we further design complex spatial reasoning question-answering to enhance the LLM’s reasoning ability that is crucial for autonomous driving decision-making. For instance, given a set of points along a road centerline, the model is asked to identify which objects lie on that lane. In another type of question, the LLM must determine the nearest object in a specified direction. We also introduce tasks involving two indicated objects (denoted by two arrows) and require the LLM to compute their 3D distance. These objects may appear within the same image but are more often captured across different camera views, compelling the model to perform true 3D spatial reasoning rather than relying on 2D pixel distances. Finally, we incorporate temporal reasoning tasks in which the LLM must not only identify an object but also predict its future position after a given time interval. Examples of spatial reasoning QAs are shown in Fig. 4(b).

All questions are generated from templates, and the answers



(a) Spatial-Perception Question-Answering



(b) Spatial-Reasoning Question-Answering

Figure 4. Examples to illustrate different question-answering pairs in SA-QA. The green dots, box, and line are highlighted only for visualization. The masked region and the red arrows are visible to the vision encoder.

are derived from the human-annotated ground-truth labels in the nuScenes dataset [2] and its extension OpenLane dataset [5]. This design fully leverages the high-precision annotations of nuScenes, guiding the model toward spatially aware understanding. More details on SA-QA dataset are provided in the supplementary material.

4. Experiments

4.1. Implementation Details

Following the configuration of our base model OmniDrive-Agent [50], we utilize EVA-02-L [13] as the vision encoder and LLaVA v1.5 [31] as the LLM, initializing the latter with its pretrained weights on the LLaVA-665K dataset [31]. For the point cloud encoder, we employ FSDv2 [12] pretrained on nuScenes [2]. We jointly finetune the entire LVLDriver—applying LoRA only to the LLM components—on the OmniDrive dataset [50] and our proposed SA-QA dataset. The learning rate for the Gradual Fusion Q-Former is set to 4×10^{-4} , while the learning rate for image encoder, point encoder and LLM is 2×10^{-5} . We use AdamW optimizer with a batch size of 16 and train for 12 epochs, using a 500-iteration warmup followed by cosine annealing policy. Training requires approximately 30 hours on 8xA100 GPUs (40 GB each). Additionally, we

finetune LVLDriver on the DriveLM dataset to evaluate its performance on DriveLM.

4.2. Dataset & Metrics

nuScenes. The nuScenes dataset [2] is a comprehensive real-world dataset for autonomous driving research, capturing across 1,000 diverse driving scenes from Boston and Singapore. Each scene is fully annotated with 3D bounding boxes, object attributes, tracking IDs, and rich metadata, making nuScenes one of the most comprehensive datasets for 3D perception and prediction. OpenLane [5] supplements the dataset with high-quality labels for lane boundaries, centerlines, and traffic lights, which enables the generation of lane related question-answering pairs. In this work, we primarily utilize the camera images and LiDAR scans from nuScenes as model inputs, and adopt the future ego-vehicle trajectories as ground truth for evaluating open-loop planning performance.

OmniDrive. The OmniDrive dataset [50] extends nuScenes by selecting planning-oriented key-frames and utilizing GPT4 and human-in-the-loop to enrich each key scene with scene description, key objects description, and reasoning over real and counterfactual trajectories. Its annotations on trajectory plausibility—covering rule violations, collision risks,

Table 1. **Comparison on nuScenes open-loop planning.** * and ** indicate not use ego status in BEV module or planner, respectively. Best results are highlighted as **first**, **second**, and **third**.

Method	L2 (m) ↓				Collision Rate (%) ↓				Intersection Rate (%) ↓			
	1s	2s	3s	Avg.	1s	2s	3s	Avg.	1s	2s	3s	Avg.
<i>End-to-end Models</i>												
UniAD [18]	0.20	0.42	0.75	0.46	0.02	0.25	0.84	0.37	0.20	1.33	3.24	1.59
VAD-Base [22]	0.17	0.34	0.60	0.37	0.04	0.27	0.67	0.33	0.21	2.13	5.06	2.47
Ego-MLP* [60]	0.15	0.32	0.59	0.35	0.00	0.27	0.85	0.37	0.27	2.52	6.60	2.93
BEV-Planner [27]	0.16	0.32	0.57	0.35	0.00	0.29	0.73	0.34	0.35	2.62	6.51	3.16
<i>Language Models</i>												
DriveVLM [47]	0.18	0.34	0.68	0.40	0.10	0.22	0.45	0.27	-	-	-	-
OmniReason [33]	0.15	0.31	0.57	0.34	0.04	0.18	0.98	0.40	0.61	2.75	6.19	3.18
Orion** [14]	0.17	0.31	0.55	0.32	0.05	0.25	0.80	0.37	-	-	-	-
OmniDrive-Agent [50]	0.14	0.29	0.55	0.33	0.00	0.13	0.78	0.30	0.56	2.48	5.96	3.00
LVLDrive (Ours)	0.13	0.26	0.49	0.29	0.02	0.16	0.57	0.25	0.53	2.03	5.22	2.59

Table 2. **Comparison on DriveLM dataset [43].** * denotes results reproduced by us. All other metrics are quoted directly from their original publications.

Method	BLEU-4 ↑	ROUGE-L ↑	CIDEr ↑
EM-VLM4AD [15]	45.36	71.98	3.20
MiniDrive [61]	50.20	73.50	3.32
MPDrive [64]	52.71	76.98	3.56
LMAD [44]	54.49	75.72	3.84
OmniDrive-Agent* [50]	55.52	72.08	15.44
LVLDrive (Ours)	59.01	73.67	21.65

and behavioral rationality—provide richer planning-oriented supervision for training LLM-based driving models.

DriveLM. The DriveLM dataset [43] formulates autonomous driving as a graph VQA task, where scene understanding and decision-making are expressed as a directed graph of QA pairs spanning perception, prediction, planning, and motion. Built on nuScenes [2], DriveLM provides 4871 keyframes annotated with multi-stage QA graphs grounded in 3D bounding boxes and multi-view images, enabling structured evaluation of reasoning across the full driving pipeline. We follow the dataset split used in EM-VLM4AD [15], employing 90% of the data for fine-tuning and evaluating on the 5% test set. For other previous works, we directly cite the results reported in their papers after confirming that they were obtained under the same setting.

Metrics. For open-loop planning on nuScenes, our model outputs six future waypoints in a question–answer format, corresponding to the next 3 seconds at 0.5-second intervals. We compute the BEV L2 distance between each predicted waypoint and the ground-truth (GT) trajectory—also known as the Displacement Error—along with the collision rate over the entire 3-second horizon. Following BEV-Planner [27], we adopt an improved collision rate—where any collision at a given step marks all subsequent steps as collisions—and additionally evaluate the intersection rate (IR) with road

boundaries, which measures whether the predicted trajectory remains within the drivable area. In addition, to assess spatial perception, we parse bounding boxes from the VLM-generated answers responding to 3D grounding questions and compute the BEV mean Intersection over Union (mIoU), a standard metric for evaluating object detection and localization quality. More details on this grounding evaluation are provided in the supplementary material. On the DriveLM dataset, we evaluate how closely the generated answers match human annotations using standard language metrics, including BLEU-4 [39], ROUGE-L [29], and CIDEr [49].

4.3. Open-loop Planning

We compare LVLDrive with state-of-the-art end-to-end planning models and LLM-based planning approaches on the nuScenes open-loop planning benchmark in Tab. 1. LVLDrive delivers competitive results and outperforms existing LLM-based approaches. Although our model lags behind end-to-end models in Intersection Rate, LLM-based approaches offer more comprehensive functionality; for instance, our model can perform scene-level question answering. Relative to our base model OmniDrive-Agent, LVLDrive achieves consistent gains across all average metrics, validating the effectiveness of the proposed fusion mechanism and spatial-aware fine-tuning strategy. These findings underscore the crucial role of accurate spatial understanding and reasoning in enabling safe and robust planning.

4.4. Results on DriveLM Dataset

Table 2 shows that LVLDrive achieves competitive performance on BLEU-4 and ROUGE-L, indicating that its generated answers are comparable in surface-level phrasing to prior vision–language driving models. Meanwhile, LVLDrive attains a CIDEr score of 21.65, substantially outperforming all baselines. Since CIDEr emphasizes content relevance, informativeness, and alignment with human-consensus keywords, this large margin suggests that

Table 3. **Ablation on Q-Former configuration, input modalities and gate variants.** CR and IR denote collision rate and intersection, respectively. The L2 metric for open-loop planning is consistently around 0.32 meters and is therefore omitted for space. The lighter unified Q-Former, when equipped with a zero-initialized gate, outperforms using two independent Q-Formers for the image and LiDAR modalities, demonstrating the effectiveness of Gradual Fusion Q-Former.

Q-Former	Modality	Zero-init. Gate	Open-loop planning		Grounding mIoU ↑
			CR (%) ↓	IR (%) ↓	
Independent	C	N/A	0.33	3.32	0.18
	L	N/A	0.39	3.26	0.17
	C+L	N/A	0.29	3.20	0.19
Unified (Ours)	C+L	No	0.40	3.45	0.17
		Single	0.30	2.99	0.21
		Multi-head	0.28	2.93	0.21

LVLDrive produces answers that better capture the key spatial cues, object attributes, and driving-relevant semantics present in human responses. Thus, while syntax overlap remains comparable across models, LVLDrive demonstrates stronger 3D scene understanding and spatial reasoning, reflecting the advantages of our proposed LiDAR injection and spatial-aware fine-tuning.

4.5. Ablation Study

Ablation on Model Configuration. In Tab. 3, we examine how different input modalities, Q-Former configuration and gating variants affect both open-loop planning and 3D grounding. The first three rows compare models using camera input only (C), LiDAR input only (L), and their combination (C+L), where image and LiDAR features are retrieved by separate Q-Formers. Adding LiDAR as an additional modality yields moderate improvements, demonstrating that it provides complementary geometric cues beneficial for both planning and grounding. However, the additional Q-Former also brings extra computation and memory consumption, making it a suboptimal solution. In the unified Q-Former setting (bottom three rows), we further investigate the impact of different gating mechanisms. The multi-head gate achieves the best overall performance, reducing collision rate from 0.40% to 0.28% and intersection rate from 3.45% to 2.93% compared to the no-gate baseline, while improving mIoU from 0.17 to 0.21. These results indicate that the proposed zero-initialized multi-head gate improves training stability, leading to more robust planning and grounding. Additionally, the lightweight unified Q-Former, when equipped with a zero-initialized gate, surpasses the separate Q-Former design, further demonstrating the effectiveness of Gradual Fusion Q-Former.

Ablation on Dataset Composition. Table 4 evaluates the contributions of different components in our SA-QA dataset

Table 4. **Ablation on dataset composition.** P. and R. stand for perception and reasoning QAs, respectively. CR and IR denote collision rate and intersection, respectively. The L2 metric for open-loop planning is consistently around 0.32 meters and is therefore omitted for space.

OmniDrive	SA-QA		Open-loop planning		Grounding
	P.	R.	CR (%) ↓	IR (%) ↓	mIoU ↑
✓			0.39	3.17	0.00
✓	✓		0.29	2.89	0.20
✓		✓	0.33	2.84	0.11
✓	✓	✓	0.27	2.83	0.22

by separating perception-oriented QAs (*e.g.* 3D grounding, drivable-area judgment) from reasoning-oriented QAs (*e.g.* estimating inter-object distances, predicting agent intentions). Interestingly, when trained solely on the OmniDrive dataset [50], LVLDrive collapses on the grounding task. Although the model can still produce seemingly reasonable textual responses, it consistently omits key information required to reconstruct a 3D box—such as size or orientation—making it impossible to parse a valid box from the output. As a result, the grounding metric drops to zero. Incorporating perception QAs notably improves all metrics, reducing the collision rate from 0.39% to 0.29% and the intersection rate from 3.17% to 2.89%. Incorporating reasoning QAs further boosts overall performance relative to training solely on OmniDrive. Nevertheless, compared with adding only perception QAs, the CR and mIoU are still inferior. We attribute this to the scarcity of reasoning questions that demand accurate 3D information about individual objects, which limits the model’s ability to learn robust instruction-following behavior. When both perception and reasoning QAs are used during training, the model achieves the best overall results, with the lowest CR (0.27%), lowest IR (2.83%), and highest mIoU (0.22). These findings demonstrate that perception and reasoning QAs offer complementary supervision signals that jointly enhance spatial understanding and decision-making.

5. Conclusion

In this work, we introduced LVLDrive, a LiDAR-Vision-Language framework that enhances Vision-Language Models (VLMs) with robust 3D metric spatial understanding for autonomous driving. By integrating LiDAR information through our Gradual Fusion Q-Former, LVLDrive effectively fuses LiDAR and image inputs while preserving the linguistic and visual reasoning capabilities of the pre-trained VLM backbone. In addition, we proposed a spatial-aware question-answering dataset that explicitly guides the model to interpret and utilize LiDAR point clouds through carefully designed QA pairs covering 3D grounding, spatial reasoning,

and future state prediction. Our experiments demonstrate the effectiveness of integrating explicit 3D spatial information into VLMs, leading to improved reasoning and decision-making in autonomous driving systems.

Limitations and Future Work. Despite the benefits of our gradual fusion strategy, LVLDrive is still constrained by the limited availability of large-scale, naturally paired text–LiDAR data. In an ideal setting, one would pretrain a unified model on large-scale aligned language–LiDAR samples, enabling the representation space of 3D geometry and linguistic concepts to be co-optimized from scratch. The construction of such datasets remains extremely challenging, and closing this gap is an important direction for future work.

References

- [1] Shuai Bai, Kejin Chen, Xuejing Liu, Jialin Wang, Wenbin Ge, Sibo Song, Kai Dang, Peng Wang, Shijie Wang, Jun Tang, et al. Qwen2. 5-vl technical report. *arXiv preprint arXiv:2502.13923*, 2025. 3
- [2] Holger Caesar, Varun Bankiti, Alex H. Lang, Sourabh Vora, Venice Erin Liong, Qiang Xu, Anush Krishnan, Yu Pan, Giancarlo Baldan, and Oscar Beijbom. nuScenes: A multimodal dataset for autonomous driving. In *CVPR*, 2020. 5, 6, 7, 1, 2
- [3] Mathilde Caron, Hugo Touvron, Ishan Misra, Hervé Jégou, Julien Mairal, Piotr Bojanowski, and Armand Joulin. Emerging properties in self-supervised vision transformers. In *ICCV*, 2021. 3
- [4] Boyuan Chen, Zhuo Xu, Sean Kirmani, Brian Ichter, Danny Driess, Pete Florence, Dorsa Sadigh, Leonidas Guibas, and Fei Xia. SpatialVLM: Endowing Vision-Language Models with Spatial Reasoning Capabilities. In *CVPR*, 2024. 3
- [5] Li Chen, Chonghao Sima, Yang Li, Zehan Zheng, Jiajie Xu, Xiangwei Geng, Hongyang Li, Conghui He, Jianping Shi, Yu Qiao, and Junchi Yan. Performer: 3d lane detection via perspective transformer and the openlane benchmark. In *European Conference on Computer Vision (ECCV)*, 2022. 6, 1, 2
- [6] Xinlei Chen, Saining Xie, and Kaiming He. An empirical study of training self-supervised vision transformers. In *ICCV*, 2021. 3
- [7] An-Chieh Cheng, Hongxu Yin, Yang Fu, Qiushan Guo, Ruihan Yang, Jan Kautz, Xiaolong Wang, and Sifei Liu. SpatialRGPT: Grounded Spatial Reasoning in Vision Language Models. In *NeurIPS*, 2024-10-15. 3
- [8] Tushar Choudhary, Vikrant Dewangan, Shivam Chandok, Shubham Priyadarshan, Anushka Jain, Arun K Singh, Siddharth Srivastava, Krishna Murthy Jatavallabhula, and K Madhava Krishna. Talk2bev: Language-enhanced bird’s-eye view maps for autonomous driving. In *2024 IEEE International Conference on Robotics and Automation (ICRA)*, pages 16345–16352. IEEE, 2024. 2
- [9] Thierry Deruyttere, Simon Vandenhende, Dusan Grujicic, Luc Van Gool, and Marie Francine Moens. Talk2car: Taking control of your self-driving car. In *Proceedings of the 2019 conference on empirical methods in natural language processing and the 9th international joint conference on natural language processing (EMNLP-IJCNLP)*, pages 2088–2098, 2019. 2
- [10] Xinpeng Ding, Jianhua Han, Hang Xu, Xiaodan Liang, Wei Zhang, and Xiaomeng Li. Holistic autonomous driving understanding by bird’s-eye-view injected multi-modal large models. In *Proceedings of the IEEE/CVF Conference on Computer Vision and Pattern Recognition*, pages 13668–13677, 2024. 2, 3
- [11] Alexey Dosovitskiy, Lucas Beyer, Alexander Kolesnikov, Dirk Weissenborn, Xiaohua Zhai, Thomas Unterthiner, Mostafa Dehghani, Matthias Minderer, Georg Heigold, Sylvain Gelly, Jakob Uszkoreit, and Neil Houlsby. An image is worth 16x16 words: Transformers for image recognition at scale. In *ICLR*, 2021. 3
- [12] Lue Fan, Feng Wang, Naiyan Wang, and Zhaoxiang Zhang. Fsd v2: Improving fully sparse 3d object detection with virtual voxels. *IEEE Transactions on Pattern Analysis and Machine Intelligence*, 2024. 6
- [13] Yuxin Fang, Quan Sun, Xinggang Wang, Tiejun Huang, Xinlong Wang, and Yue Cao. Eva-02: A visual representation for neon genesis. *Image and Vision Computing*, page 105171, 2024. 6
- [14] Haoyu Fu, Diankun Zhang, Zongchuang Zhao, Jianfeng Cui, Dingkang Liang, Chong Zhang, Dingyuan Zhang, Hongwei Xie, Bing Wang, and Xiang Bai. ORION: A Holistic End-to-End Autonomous Driving Framework by Vision-Language Instructed Action Generation. In *ICCV*, 2025. 7
- [15] Akshay Gopalkrishnan, Ross Greer, and Mohan Trivedi. Multi-Frame, Lightweight & Efficient Vision-Language Models for Question Answering in Autonomous Driving. In *CVPRw*, 2024. 7
- [16] Kaiming He, Georgia Gkioxari, Piotr Dollár, and Ross Girshick. Mask r-cnn. In *Proceedings of the IEEE international conference on computer vision*, pages 2961–2969, 2017. 3
- [17] Kaiming He, Xinlei Chen, Saining Xie, Yanghao Li, Piotr Dollár, and Ross Girshick. Masked autoencoders are scalable vision learners. In *CVPR*, 2021. 3
- [18] Yihan Hu, Jiazhi Yang, Li Chen, Keyu Li, Chonghao Sima, Xizhou Zhu, Siqi Chai, Senyao Du, Tianwei Lin, Wenhai Wang, et al. Planning-oriented autonomous driving. In *Proceedings of the IEEE/CVF conference on computer vision and pattern recognition*, pages 17853–17862, 2023. 7
- [19] Yidong Huang, Jacob Sansom, Ziqiao Ma, Felix Gervits, and Joyce Chai. Drivlme: Enhancing llm-based autonomous driving agents with embodied and social experiences. In *2024 IEEE/RSJ International Conference on Intelligent Robots and Systems (IROS)*, pages 3153–3160. IEEE, 2024. 3
- [20] Aaron Hurst, Adam Lerer, Adam P Goucher, Adam Perelman, Aditya Ramesh, Aidan Clark, AJ Ostrow, Akila Welihinda, Alan Hayes, Alec Radford, et al. Gpt-4o system card. *arXiv preprint arXiv:2410.21276*, 2024. 3
- [21] Mengdi Jia, Zekun Qi, Shaochen Zhang, Wenyao Zhang, Xinqiang Yu, Jiawei He, He Wang, and Li Yi. Omnispatial: Towards comprehensive spatial reasoning benchmark for vision language models. *arXiv preprint arXiv:2506.03135*, 2025. 3
- [22] Bo Jiang, Shaoyu Chen, Qing Xu, Bencheng Liao, Jiajie Chen, Helong Zhou, Qian Zhang, Wenyu Liu, Chang Huang, and

Xinggang Wang. Vad: Vectorized scene representation for efficient autonomous driving. In *Proceedings of the IEEE/CVF International Conference on Computer Vision*, pages 8340–8350, 2023. 7

[23] Jinkyu Kim, Anna Rohrbach, Trevor Darrell, John Canny, and Zeynep Akata. Textual explanations for self-driving vehicles. In *Proceedings of the European conference on computer vision (ECCV)*, pages 563–578, 2018. 2

[24] Boyi Li, Yue Wang, Jiageng Mao, Boris Ivanovic, Sushant Veer, Karen Leung, and Marco Pavone. Driving everywhere with large language model policy adaptation. In *Proceedings of the IEEE/CVF Conference on Computer Vision and Pattern Recognition*, pages 14948–14957, 2024. 1, 3

[25] Junnan Li, Dongxu Li, Caiming Xiong, and Steven Hoi. Blip: Bootstrapping language-image pre-training for unified vision-language understanding and generation. In *ICML*, 2022. 3

[26] Junnan Li, Dongxu Li, Silvio Savarese, and Steven Hoi. Blip-2: bootstrapping language-image pre-training with frozen image encoders and large language models. In *ICML*, 2023. 3

[27] Zhiqi Li, Zhiding Yu, Shiyi Lan, Jiahua Li, Jan Kautz, Tong Lu, and Jose M. Alvarez. Is ego status all you need for open-loop end-to-end autonomous driving? In *CVPR*, 2024. 7

[28] Tingting Liang, Hongwei Xie, Kaicheng Yu, Zhongyu Xia, Zhiwei Lin, Yongtao Wang, Tao Tang, Bing Wang, and Zhi Tang. Bevfusion: A simple and robust lidar-camera fusion framework. In *Advances in Neural Information Processing Systems*, 2022. 2

[29] Chin-Yew Lin. Rouge: A package for automatic evaluation of summaries. In *ACL Workshop*, 2004. 7

[30] Haotian Liu, Chunyuan Li, Qingyang Wu, and Yong Jae Lee. Visual instruction tuning. *Advances in neural information processing systems*, 36:34892–34916, 2023. 3

[31] Haotian Liu, Chunyuan Li, Yuheng Li, and Yong Jae Lee. Improved baselines with visual instruction tuning. In *CVPR*, 2024-05-15. 3, 6

[32] Jingping Liu, Ziyan Liu, Zhedong Cen, Yan Zhou, Yinan Zou, Weiyan Zhang, Haiyun Jiang, and Tong Ruan. Can multi-modal large language models understand spatial relations? *arXiv preprint arXiv:2505.19015*, 2025. 3

[33] Pei Liu, Qingtian Ning, Xinyan Lu, Haipeng Liu, Weiliang Ma, Dangen She, Peng Jia, Xianpeng Lang, and Jun Ma. Omnidreason: A temporal-guided vision-language-action framework for autonomous driving. *arXiv preprint arXiv:2509.00789*, 2025. 7

[34] Wufei Ma, Haoyu Chen, Guofeng Zhang, Yu-Cheng Chou, Jieneng Chen, Celso de Melo, and Alan Yuille. 3dsrbench: A comprehensive 3d spatial reasoning benchmark. In *Proceedings of the IEEE/CVF International Conference on Computer Vision*, pages 6924–6934, 2025. 3

[35] Jiageng Mao, Yuxi Qian, Junjie Ye, Hang Zhao, and Yue Wang. Gpt-driver: Learning to drive with gpt. *arXiv preprint arXiv:2310.01415*, 2023. 3

[36] Ana-Maria Marcu, Long Chen, Jan Hünermann, Alice Karnsund, Benoit Hanotte, Prajwal Chidananda, Saurabh Nair, Vijay Badrinarayanan, Alex Kendall, Jamie Shotton, et al. Lingoqa: Visual question answering for autonomous driving. In *European Conference on Computer Vision*, pages 252–269. Springer, 2024. 2

[37] Long Ouyang, Jeffrey Wu, Xu Jiang, Diogo Almeida, Carroll Wainwright, Pamela Mishkin, Chong Zhang, Sandhini Agarwal, Katarina Slama, Alex Ray, et al. Training language models to follow instructions with human feedback. *Advances in neural information processing systems*, 35:27730–27744, 2022. 3

[38] Chenbin Pan, Burhaneddin Yaman, Tommaso Nesti, Abhirup Mallik, Alessandro G Allievi, Senem Velipasalar, and Liu Ren. Vlp: Vision language planning for autonomous driving. In *Proceedings of the IEEE/CVF Conference on Computer Vision and Pattern Recognition*, pages 14760–14769, 2024. 1, 2

[39] Kishore Papineni, Salim Roukos, Todd Ward, and Wei-Jing Zhu. Bleu: a method for automatic evaluation of machine translation. In *ACL*, 2002. 7

[40] Tianwen Qian, Jingjing Chen, Linhai Zhuo, Yang Jiao, and Yu-Gang Jiang. Nuscenes-qa: A multi-modal visual question answering benchmark for autonomous driving scenario. In *Proceedings of the AAAI Conference on Artificial Intelligence*, pages 4542–4550, 2024. 2

[41] Alec Radford, Jong Wook Kim, Chris Hallacy, Aditya Ramesh, Gabriel Goh, Sandhini Agarwal, Girish Sastry, Amanda Askell, Pamela Mishkin, Jack Clark, Gretchen Krueger, and Ilya Sutskever. Learning transferable visual models from natural language supervision. In *ICML*, 2022. 3

[42] Hao Shao, Yuxuan Hu, Letian Wang, Guanglu Song, Steven L Waslander, Yu Liu, and Hongsheng Li. Lmdrive: Closed-loop end-to-end driving with large language models. In *Proceedings of the IEEE/CVF Conference on Computer Vision and Pattern Recognition*, pages 15120–15130, 2024. 1, 2

[43] Chonghao Sima, Katrin Renz, Kashyap Chitta, Li Chen, Hanxue Zhang, Chengan Xie, Jens Beißenwenger, Ping Luo, Andreas Geiger, and Hongyang Li. Drivelm: Driving with graph visual question answering. In *European conference on computer vision*, pages 256–274. Springer, 2024. 1, 2, 7

[44] Nan Song, Bozhou Zhang, Xiatian Zhu, Jiankang Deng, and Li Zhang. LMAD: Integrated end-to-end vision-language model for Explainable Autonomous Driving. *arXiv preprint: 2508.12404*, 2025. 7

[45] Tao Tang, Dafeng Wei, Zhengyu Jia, Tian Gao, Changwei Cai, Chengkai Hou, Peng Jia, Kun Zhan, Haiyang Sun, Fan JingChen, et al. Bev-tsr: Text-scene retrieval in bev space for autonomous driving. In *Proceedings of the AAAI Conference on Artificial Intelligence*, pages 7275–7283, 2025. 2

[46] Kexin Tian, Jingrui Mao, Yunlong Zhang, Jiwan Jiang, Yang Zhou, and Zhengzhong Tu. NuScenes-SpatialQA: A Spatial Understanding and Reasoning Benchmark for Vision-Language Models in Autonomous Driving. In *ICCVw*, 2025. 1, 2, 3

[47] Xiaoyu Tian, Junru Gu, Bailin Li, Yicheng Liu, Yang Wang, Zhiyong Zhao, Kun Zhan, Peng Jia, Xianpeng Lang, and Hang Zhao. Drivevlm: The convergence of autonomous driving and large vision-language models. In *Conference on Robot Learning (CoRL)*, 2024. 3, 7

[48] Hugo Touvron, Thibaut Lavril, Gautier Izacard, Xavier Martinet, Marie-Anne Lachaux, Timothée Lacroix, Baptiste

Rozière, Naman Goyal, Eric Hambro, Faisal Azhar, et al. Llama: Open and efficient foundation language models. *arXiv preprint arXiv:2302.13971*, 2023. 3

[49] Ramakrishna Vedantam, C. Lawrence Zitnick, and Devi Parikh. Cider: Consensus-based image description evaluation. In *CVPR*, 2015. 7

[50] Shihao Wang, Zhiding Yu, Xiaohui Jiang, Shiyi Lan, Min Shi, Nadine Chang, Jan Kautz, Ying Li, and Jose M Alvarez. Omnidrive: A holistic vision-language dataset for autonomous driving with counterfactual reasoning. In *Proceedings of the Computer Vision and Pattern Recognition Conference*, pages 22442–22452, 2025. 2, 3, 6, 7, 8

[51] Zitian Wang, Zehao Huang, Yulu Gao, Naiyan Wang, and Si Liu. Mv2dfusion: Leveraging modality-specific object semantics for multi-modal 3d detection. In *IEEE Transactions on Pattern Analysis and Machine Intelligence*, 2025. 2

[52] Zhiyu Wu, Xiaokang Chen, Zizheng Pan, Xingchao Liu, Wen Liu, Damai Dai, Huazuo Gao, Yiyang Ma, Chengyue Wu, Bingxuan Wang, et al. Deepseek-vl2: Mixture-of-experts vision-language models for advanced multimodal understanding. *arXiv preprint arXiv:2412.10302*, 2024. 3

[53] Enze Xie, Wenhui Wang, Zhiding Yu, Anima Anandkumar, Jose M Alvarez, and Ping Luo. Segformer: Simple and efficient design for semantic segmentation with transformers. *Advances in neural information processing systems*, 34:12077–12090, 2021. 3

[54] Qingyao Xu, Siheng Chen, Guang Chen, Yanfeng Wang, and Ya Zhang. Chatbev: A visual language model that understands bev maps. *arXiv preprint arXiv:2503.13938*, 2025. 2

[55] Yiran Xu, Xiaoyin Yang, Lihang Gong, Hsuan-Chu Lin, Tz-Ying Wu, Yunsheng Li, and Nuno Vasconcelos. Explainable object-induced action decision for autonomous vehicles. In *Proceedings of the IEEE/CVF Conference on Computer Vision and Pattern Recognition*, pages 9523–9532, 2020. 2

[56] Zhenhua Xu, Yujia Zhang, Enze Xie, Zhen Zhao, Yong Guo, Kwan-Yee K Wong, Zhenguo Li, and Hengshuang Zhao. Drivegpt4: Interpretable end-to-end autonomous driving via large language model. *IEEE Robotics and Automation Letters*, 2024. 3

[57] Jihan Yang, Shusheng Yang, Anjali W Gupta, Rilyn Han, Li Fei-Fei, and Saining Xie. Thinking in space: How multimodal large language models see, remember, and recall spaces. In *Proceedings of the Computer Vision and Pattern Recognition Conference*, pages 10632–10643, 2025. 1, 3

[58] Senqiao Yang, Jiaming Liu, Renrui Zhang, Mingjie Pan, Ziyu Guo, Xiaoqi Li, Zehui Chen, Peng Gao, Hongsheng Li, Yandong Guo, et al. Lidar-llm: Exploring the potential of large language models for 3d lidar understanding. In *Proceedings of the AAAI Conference on Artificial Intelligence*, pages 9247–9255, 2025. 3

[59] Junwei You, Haotian Shi, Zhuoyu Jiang, Zilin Huang, Rui Gan, Keshu Wu, Xi Cheng, Xiaopeng Li, and Bin Ran. V2x-vlm: End-to-end v2x cooperative autonomous driving through large vision-language models. *arXiv preprint arXiv:2408.09251*, 2024. 3

[60] Jiang-Tian Zhai, Ze Feng, Jinhao Du, Yongqiang Mao, Jiang-Jiang Liu, Zichang Tan, Yifu Zhang, Xiaoqing Ye, and Jing-dong Wang. Rethinking the open-loop evaluation of end-to-end autonomous driving in nuscenes. *arXiv preprint arXiv:2305.10430*, 2023. 7

[61] Enming Zhang, Xingyuan Dai, Min Huang, Yisheng Lv, and Qinghai Miao. MiniDrive: More Efficient Vision-Language Models with Multi-Level 2D Features as Text Tokens for Autonomous Driving. *arXiv preprint: 2409.07267*, 2025-05-21. 7

[62] Renrui Zhang, Jiaming Han, Chris Liu, Peng Gao, Aojun Zhou, Xiangfei Hu, Shilin Yan, Pan Lu, Hongsheng Li, and Yu Qiao. LLaMA-Adapter: Efficient Fine-tuning of language models with Zero-init Attention. In *ICLR*, 2024. 4

[63] Ye Zhang and Yiming Nie. Interndrive: A multimodal large language model for autonomous driving scenario understanding. In *Proceedings of the 2024 4th International Conference on Artificial Intelligence, Automation and High Performance Computing*, pages 294–305, 2024. 3

[64] Zhiyuan Zhang, Xiaofan Li, Zhihao Xu, Wenjie Peng, Zijian Zhou, Miaojing Shi, and Shuangping Huang. MPDrive: Improving spatial understanding with Marker-Based Prompt Learning for Autonomous Driving. In *CVPR*, 2025. 7

[65] Xingcheng Zhou, Xuyuan Han, Feng Yang, Yunpu Ma, and Alois C Knoll. Opendrivevla: Towards end-to-end autonomous driving with large vision language action model. *arXiv preprint arXiv:2503.23463*, 2025. 3

[66] Zewei Zhou, Tianhui Cai, Seth Z Zhao, Yun Zhang, Zhiyu Huang, Bolei Zhou, and Jiaqi Ma. Autovla: A vision-language-action model for end-to-end autonomous driving with adaptive reasoning and reinforcement fine-tuning. In *NeurIPS*, 2025. 3

Spatial-aware Vision Language Model for Autonomous Driving

Supplementary Material

6. Abstract

This supplementary material provides additional details and analyses of our work. Further information about our proposed SA-QA dataset is presented in Sec. 7, and a detailed comparison with NuScenes-SpatialQA is provided in Sec. 8. Additional details on the 3D grounding benchmark are included in Sec. 9.

7. More Details on SA-QA Dataset

This dataset is built on top of nuScenes [2] and enriched using the ground-truth annotations provided by both nuScenes and OpenLane [5] to generate question-answering (QA) pairs. The specific QA formats and the step-by-step generation procedure are summarized in Tab. 5 and Tab. 6. Note that before generating any QA pairs, we convert all annotations and LiDAR point clouds into the ego coordinate system.

8. Comparison with NuScenes-SpatialQA

NuScenes-SpatialQA [46] is a concurrent study that shares certain similarities with our proposed SA-QA dataset. While both datasets focus on the spatial reasoning of Vision-Language Models (VLMs), SA-QA diverges by prioritizing instruction tuning, explicit metric grounding, and cross-modal alignment.

Training vs. Evaluation Focus. NuScenes-SpatialQA is constructed exclusively on the nuScenes validation split (150 scenes). Its primary purpose is to serve as a zero-shot benchmark to evaluate existing general-purpose VLMs. In contrast, SA-QA is designed as a massive-scale instruction-tuning dataset constructed on the training split (850 scenes). This scale allows LVLDrive to learn complex spatial relationships rather than merely being tested on them.

Enhanced Cross-Modality Interaction. To promote robust alignment across modalities, SA-QA introduces specific task designs targeting Text-Vision-LiDAR integration. We implement modality masking (Tab. 5, SP-04), which masks the target in the image to encourage the model to retrieve geometric information directly from the LiDAR data. Furthermore, we utilize visual cues (Tab. 5, SP-03; Tab. 6, SR-03), where prompts explicitly reference arrows drawn on the image. This design drives the model to bind language with joint image-LiDAR features, enabling richer 2D-3D spatial reasoning.

Explicit 3D Grounding vs. Relative Depth. While NuScenes-SpatialQA utilizes 3D annotations to generate

answers, its questions are largely limited to relative 3D distances or topological relationships (*e.g.* “Is object A closer than object B?”), omitting explicit 3D locations. This allows models to rely on approximate depth cues without mastering metric space. Conversely, SA-QA dataset requires explicit 3D grounding, asking the model to output precise coordinates (x, y) and absolute dimensions (Tab. 5, SP-02). This forces the model to internalize a true metric understanding of the 3D environment.

Global Perception vs. Intra-View Limitations. A critical limitation of NuScenes-SpatialQA is that questions are typically restricted to the same camera view. This relies on local visual comparisons and omits a holistic perception of the surrounding environment. SA-QA explicitly challenges this by constructing cross-view reasoning tasks (Tab. 6, SR-03) where target objects may appear in disparate sensors (*e.g.* Front Camera vs. Back-Right Camera). To answer these correctly, the model cannot rely on a single 2D image but must fuse information into a unified global coordinate system.

Automated Efficiency vs. LLM Latency. NuScenes-SpatialQA relies on heavy Large Language Models to generate dense captions and formulate questions, a process that introduces significant computational latency and cost. In contrast, SA-QA is fully automated and rule-based. By deriving QA pairs directly from ground-truth annotations, our generation process is computationally negligible. This high efficiency supports dynamic augmentation, allowing us to apply random sampling strategies on the fly—specifically randomizing target objects, lane segments, and temporal intervals for future prediction.

9. More Details on 3D Grounding Benchmark

Throughout model development, we observed that planning-only evaluation is insufficient and fails to capture a model’s understanding of the spatial distribution of surrounding objects. To better assess this capability, we construct a grounding benchmark using the ground-truth annotations of the nuScenes nuscenes validation set.

Distance-Based Object Sampling. Traversing all annotated objects would lead to prohibitive inference time, so we sample target objects based on distance. For each frame, we compute the distance from the bottom center of every annotated 3D bounding box to the ego vehicle and sort all objects by distance. The objects are then grouped into four ranges. After experimenting with interval sizes of 15 m, 20 m, and 25 m, we found that a 15 m step yields the most balanced distribution across groups, and thus adopt 15 m as the inter-

Table 5. Generation logic for spatial perception (SP) tasks in the SA-QA dataset.

ID	Prompt Template	Input Data Transformation	Generation Logic	Answer Generation
SP-01	“For a potential future position at (x, y) , is it in a drivable area?”	None.	<ol style="list-style-type: none"> 1. Randomly sample a query point in the front region of the ego-vehicle ($5 \leq X \leq 20, -5 \leq Y \leq 5$). 2. Generate a drivable mask in BEV by buffering lane centerlines with a 1.75m margin. 3. Check point inclusion against the mask. 	Binary: “Yes” if inside; “No” otherwise.
SP-02	“Identify the object in $\langle CAM, x_{min}, y_{min}, x_{max}, y_{max} \rangle$ and describe its 3D information.”	None.	<ol style="list-style-type: none"> 1. Project 3D annotations to the 2D planes of all 6 cameras. 2. Compute 2D bounding boxes $[x_{min}, y_{min}, x_{max}, y_{max}]$ clamped to image dims, filtering out candidates that are invisible or too small. 3. Sample an object and format the answer. 4. Format the prompt with the target object’s coordinates. 	Text: “The object is a $\langle \text{category} \rangle$ in the $\langle CAM \rangle$, location: (x, y) , length: $\langle l \rangle$, width: $\langle w \rangle$, height: $\langle h \rangle$, angles in degree: $\langle yaw \rangle$. (Rounded to 0.1).”
SP-03	“Identify the object cued by the arrow and describe its 3D information.”	Draw an arrow on the image.	<ol style="list-style-type: none"> 1–3. Follow steps 1–3 of SP-02 to filter candidates and sample one object. 4. Draw a visual arrow on the image pointing to the center of the target’s 2D mask. 5. Construct the prompt referencing the arrow cue. 	Text: Same format as SP-02.
SP-04	“Identify the object in the masked region and describe its 3D information.”	Mask a region of the image.	<ol style="list-style-type: none"> 1–3. Follow steps 1–3 of SP-02 to filter candidates and sample one object. 4. Apply a mask to the target’s 2D bounding box region (forcing LiDAR reliance). 5. Construct the prompt referencing the masked region. 	Text: Same format as SP-02.

Table 6. Generation logic for spatial reasoning (SR) tasks in the SA-QA dataset.

ID	Prompt Template	Input Data Transformation	Generation Logic	Answer Generation
SR-01	“What objects are on the lane defined by points $(x_1, y_1), (x_2, y_2), (x_3, y_3)$?”	None.	<ol style="list-style-type: none"> 1. Randomly select a lane centerline from the OpenLane [5] map annotations. 2. Aggregate the associated objects located on the selected lane centerline from the OpenLane annotation set [5]. 3. Format the prompt and answer. 	List: “The object is a $\langle \text{category} \rangle$, location...”.
SR-02	“What is the nearest object in the $\langle \text{DIRECTION} \rangle$ direction?”	None.	<ol style="list-style-type: none"> 1. Define 4 spatial sectors (e.g. Front-Left, Back-Left) relative to the current ego-vehicle heading. 2. Filter objects located within the target area. 3. Calculate Euclidean distances for all candidates and sort in ascending order. 4. Format the prompt and answer. 	Text: Description of the object with index 0 (minimum distance), using the format from SP-02.
SR-03	“Please determine the metric distance (in meters) separating the two indicated objects.”	Draw arrows on the images.	<ol style="list-style-type: none"> 1. Select two distinct visible objects (O_A, O_B), potentially across different camera views. 2. Draw visual arrows pointing to O_A and O_B in their respective images (following SP-03). 3. Compute the L2 norm between their 3D centroids: $\ C_A - C_B\ _2$. 	Scalar: “ D .” (The value is rounded to 0.1 meters).
SR-04	“What is the future position of the object at (x, y) after T second?”	None.	<ol style="list-style-type: none"> 1. Randomly sample one object that possesses a future trajectory within the nuScenes annotation set [2]. 2. Randomly select a future position and time interval for the sampled object, and subsequently structure the input prompt and the corresponding target answer. 	Coordinate: “ (x_{fut}, y_{fut}) .”

Table 7. Distribution of object counts across distance ranges in our grounding benchmark.

0-15m	15-30m	30-45m	45m-Inf	Overall
5,304	5,684	5,367	3,903	20,258

val. Finally, for each frame, we randomly sample one object from each distance range to form our grounding benchmark. The number of objects in each range is shown in Tab. 7.

Question and Answer Generation. For each selected object, we format its 3D bounding box parameters using the following answer template: The object is a *<class>* in the *<direction>*, location: (X, Y) , length: L , width: W , height: H , angles in degrees: θ . Meanwhile, we project the eight corners of the 3D box onto the image plane and compute the corresponding 2D bounding box $(x_{min}, y_{min}, x_{max}, y_{max})$, which is incorporated into the question. If any of these coordinates fall outside the image bounds, they are clipped to the valid image range.

Answer Parsing and Evaluation. Because similar QA patterns are also used during training, the model typically produces answers that closely follow the desired template. This allows us to reliably parse a BEV bounding box (X, Y, L, W, θ) from the predicted answer and compute the BEV mIoU. Concretely, we first compute the IoU for each individual object. We then average the IoUs within each of the four distance ranges, and finally report the mean of these four group-wise IoUs as the overall grounding metric.